

Limiting neutrino magnetic moments with Borexino Phase-II solar neutrino data

M. Agostini,¹ K. Altenmüller,² S. Appel,² V. Atroshchenko,³ Z. Bagdasarian,⁴ D. Basilico,⁵ G. Bellini,⁵ J. Benziger,⁶ D. Bick,⁷ G. Bonfini,⁸ D. Bravo,⁹ B. Caccianiga,⁵ F. Calaprice,¹⁰ A. Caminata,¹¹ S. Caprioli,⁵ M. Carlini,⁸ P. Cavalcante,^{8,9} A. Chepurinov,¹² K. Choi,¹³ L. Collica,⁵ D. D'Angelo,⁵ S. Davini,¹¹ A. Derbin,¹⁴ X.F. Ding,¹ A. Di Ludovico,¹⁰ L. Di Noto,¹¹ I. Drachnev,^{1,14} K. Fomenko,¹⁵ A. Formozov,^{16,5,17} D. Franco,¹⁸ F. Froberg,¹⁰ F. Gabriele,⁸ C. Galbiati,¹⁰ C. Ghiano,⁸ M. Giammarchi,⁵ A. Goretti,¹⁰ M. Gromov,¹⁷ D. Guffanti,⁷ C. Hagner,⁷ T. Houdy,¹⁸ E. Hungerford,¹⁹ Aldo Ianni,^{8,20} Andrea Ianni,¹⁰ A. Jany,²¹ D. Jeschke,² V. Kobychyev,²² D. Korablev,¹⁵ G. Korga,¹⁹ D. Kryn,¹⁸ M. Laubenstein,⁸ E. Litvinovich,^{3,23} F. Lombardi,^{8,24} P. Lombardi,⁵ L. Ludhova,^{4,25} G. Lukyanchenko,³ L. Lukyanchenko,³ I. Machulin,^{3,23} G. Manuzio,¹¹ S. Maccocci,^{1,11} J. Martyn,²⁶ E. Meroni,⁵ M. Meyer,²⁷ L. Miramonti,⁵ M. Misiaszek,²¹ V. Muratova,¹⁴ B. Neumair,² L. Oberauer,² B. Opitz,⁷ V. Orekhov,³ F. Ortica,²⁸ M. Pallavicini,¹¹ L. Papp,² Ö. Penek,^{4,25} N. Pilipenko,¹⁴ A. Pocar,²⁹ A. Porcelli,²⁶ G. Ranucci,⁵ A. Razeto,⁸ A. Re,⁵ M. Redchuk,^{4,25} A. Romani,²⁸ R. Roncin,^{8,18} N. Rossi,⁸ S. Schönert,² D. Semenov,¹⁴ M. Skorokhvatov,^{3,23} O. Smirnov,¹⁵ A. Sotnikov,¹⁵ L.F.F. Stokes,⁸ Y. Suvorov,^{30,3} R. Tartaglia,⁸ G. Testera,¹¹ J. Thurn,²⁷ M. Toropova,³ E. Unzhakov,¹⁴ A. Vishneva,¹⁵ R.B. Vogelaar,⁹ F. von Feilitzsch,² H. Wang,³⁰ S. Weinz,²⁶ M. Wojcik,²¹ M. Wurm,²⁶ Z. Yokley,⁹ O. Zaimidoroga,¹⁵ S. Zavatarelli,¹¹ K. Zuber,²⁷ and G. Zuzel²¹

(The Borexino collaboration)

¹Gran Sasso Science Institute (INFN), 67100 L'Aquila, Italy

²Physik-Department and Excellence Cluster Universe,

Technische Universität München, 85748 Garching, Germany

³National Research Centre Kurchatov Institute, 123182 Moscow, Russia

⁴Institut für Kernphysik, Forschungszentrum Jülich, 52425 Jülich, Germany

⁵Dipartimento di Fisica, Università degli Studi e INFN, 20133 Milano, Italy

⁶Chemical Engineering Department, Princeton University, Princeton, NJ 08544, USA

⁷Institut für Experimentalphysik, Universität Hamburg, 22761 Hamburg, Germany

⁸INFN Laboratori Nazionali del Gran Sasso, 67010 Assergi (AQ), Italy

⁹Physics Department, Virginia Polytechnic Institute and State University, Blacksburg, VA 24061, USA

¹⁰Physics Department, Princeton University, Princeton, NJ 08544, USA

¹¹Dipartimento di Fisica, Università degli Studi e INFN, 16146 Genova, Italy

¹²Moscow State University Skobeltsyn Institute of Nuclear Physics, 119234 Moscow, Russia

¹³Department of Physics and Astronomy, University of Hawaii, Honolulu, HI 96822, USA

¹⁴St. Petersburg Nuclear Physics Institute NRC Kurchatov Institute, 188350 Gatchina, Russia

¹⁵Joint Institute for Nuclear Research, 141980 Dubna, Russia

¹⁶Joint Institute for Nuclear Research, 141980 Dubna, Russia special symbols

¹⁷Lomonosov Moscow State University Skobeltsyn Institute of Nuclear Physics, 119234 Moscow, Russia

¹⁸AstroParticule et Cosmologie, Université Paris Diderot,

CNRS/IN2P3, CEA/IRFU, Observatoire de Paris,

Sorbonne Paris Cité, 75205 Paris Cedex 13, France

¹⁹Department of Physics, University of Houston, Houston, TX 77204, USA

²⁰Also at: Laboratorio Subterráneo de Canfranc,

Paseo de los Ayerbe S/N, 22880 Canfranc Estacion Huesca, Spain

²¹M. Smoluchowski Institute of Physics, Jagiellonian University, 30059 Krakow, Poland

²²Kiev Institute for Nuclear Research, 03680 Kiev, Ukraine

²³National Research Nuclear University MEPhI (Moscow Engineering Physics Institute), 115409 Moscow, Russia

²⁴Present address: Physics Department, University of California, San Diego, CA 92093, USA

²⁵RWTH Aachen University, 52062 Aachen, Germany

²⁶Institute of Physics and Excellence Cluster PRISMA,

Johannes Gutenberg-Universität Mainz, 55099 Mainz, Germany

²⁷Department of Physics, Technische Universität Dresden, 01062 Dresden, Germany

²⁸Dipartimento di Chimica, Biologia e Biotecnologie,

Università degli Studi e INFN, 06123 Perugia, Italy

²⁹Amherst Center for Fundamental Interactions and Physics Department,

University of Massachusetts, Amherst, MA 01003, USA

³⁰Physics and Astronomy Department, University of California Los Angeles (UCLA), Los Angeles, California 90095, USA

A search for the solar neutrino effective magnetic moment has been performed using data from 1291.5 days exposure during the second phase of the Borexino experiment. No significant deviations from the expected shape of the electron recoil spectrum from solar neutrinos have been found, and a new upper limit on the effective neutrino magnetic moment of $\mu_\nu^{eff} < 2.8 \cdot 10^{-11} \mu_B$ at 90% c.l. has been set using constraints on the sum of the solar neutrino fluxes implied by the radiochemical gallium experiments. Using the limit for the effective neutrino moment, new limits for the magnetic

moments of the neutrino flavor states, and for the elements of the neutrino magnetic moments matrix for Dirac and Majorana neutrinos, are derived.

PACS numbers: 14.60.S, 96.60.J, 26.65, 13.10

Keywords: solar neutrinos, magnetic moment

I. INTRODUCTION

Neutrinos produced in the Sun are a unique source of information with regards to their physical properties. Besides the study of well-established neutrino oscillations they can also be used to look for an anomalous magnetic moment and other electromagnetic properties of neutrinos [1]–[6]. The neutrino magnetic moment in the standard electroweak theory (SM), when extended to include neutrino mass, is proportional to the neutrino mass [7]–[12]:

$$\mu_\nu = \frac{3m_e G_F}{4\pi^2 \sqrt{2}} m_\nu \mu_B \approx 3.2 \times 10^{-19} \left(\frac{m_\nu}{1eV} \right) \mu_B, \quad (1)$$

where $\mu_B = \frac{eh}{4\pi m_e}$ is the Bohr magneton, m_e is the electron mass, and G_F is the Fermi coupling constant. The known upper limit on the neutrino masses m_ν leads to μ_ν less than $10^{-18} \mu_B$, which is roughly eight orders of magnitude lower than existing experimental limits. The most stringent laboratory bounds on μ_ν are obtained by studying (ν, e) elastic-scattering of solar neutrinos and reactor anti-neutrinos. The Super-Kamiokande Collaboration achieved a limit of $3.6 \cdot 10^{-10} \mu_B$ (90% C.L.) by fitting day/night solar neutrino spectra above 5-MeV. With additional information from other solar neutrino and KamLAND experiments a limit of $1.1 \cdot 10^{-10} \mu_B$ (90% C.L.) was obtained [13]. The Borexino collaboration reported the best current limit on the effective magnetic moment of $5.4 \cdot 10^{-11} \mu_B$ (90% C.L.) using the electron recoil spectrum from ${}^7\text{Be}$ solar neutrinos [14].

The best magnetic moment limit from reactor anti-neutrinos is $2.9 \cdot 10^{-11} \mu_B$ (90% C.L.) [15]. The most stringent limits on the neutrino magnetic moment of up to $\sim 10^{-12} \mu_B$ come from astrophysical observations [16, 17]. The complete historical record of limits on the neutrino magnetic moment can be found in [18].

Though experimental bounds on μ_ν are far from the value predicted by the extended SM, in more general models, for example with right-handed bosons or with an extended sector of scalar particles, the magnetic moment can be proportional to the mass of charged leptons and can have values close to the experimental limits reported. In more general models the proportionality between the neutrino mass and its magnetic moment doesn't hold.

In this paper, we report a search for neutrino magnetic moments using 1270.6 days of data collected during the Borexino Phase-II campaign. Borexino is the first real-time detector of low energy solar neutrinos, located in the Gran Sasso National Laboratory, Italy. Borexino detects solar neutrinos via the elastic scattering of neutrinos off

electrons in liquid scintillator. The scattered recoil electrons are detected via scintillation light, which carries the energy and position information. The mass of the scintillator (PC+PPO) is 278 tons. Events are selected within a fiducial volume (FV) corresponding to approximately 1/4 of the scintillator volume in order to provide an "active shield" against external backgrounds. Detailed descriptions of the detector can be found in [19, 20].

Neutrino-electron elastic scattering is the most sensitive test for a neutrino magnetic moment search. In the SM, the scattering of a neutrino with a non-zero magnetic moment is determined by both a weak interaction and a single-photon exchange term. The latter changes the helicity of the final neutrino state. This means that the amplitudes of the weak and electromagnetic scattering do not interfere, at least at the level of $\sim m_\nu/E_\nu$, and the total cross section is the sum of the two.

Neutrino mixing means that the coupling of the neutrino mass eigenstates i and j to an electromagnetic field is characterized by a 3×3 matrix of the magnetic (and electric) dipole moments μ_{ij} . For Majorana neutrinos the matrix μ_{ij} is anti-symmetric and only transition moments are allowed, while for Dirac neutrinos μ_{ij} is a general 3×3 matrix. The electromagnetic contribution to the ν - e scattering cross section is proportional to the square of the effective magnetic moment μ_{eff} :

$$\frac{d\sigma_{EM}}{dT_e}(T_e, E_\nu) = \pi r_0^2 \mu_{eff}^2 \left(\frac{1}{T_e} - \frac{1}{E_\nu} \right), \quad (2)$$

where μ_{eff} is measured in μ_B units and depends on the components of the neutrino moments matrix μ_{ij} , T_e is electron recoil energy, and $r_0 = 2.818 \times 10^{-13}$ cm is the classical electron radius.

The energy dependence for the magnetic and weak scattering cross sections differ significantly; for $T_e \ll E_\nu$ their ratio is proportional to $1/T_e$ and the sensitivity of the experiment to the magnetic moment strongly depends on the threshold of detection. This makes the low energy threshold of Borexino suitable for a neutrino magnetic moment search.

II. DATA SELECTION AND ANALYSIS

The data used for the analysis was collected from December 14, 2011 to May 21, 2016 with a live-time of 1291.5 days. Events were selected following the procedure optimized for the new solar neutrino analysis [21]: all events within 2 ms of any muon were rejected, whilst a dead time of 300 ms was applied after muons crossing

the inner detector; decays due to radon daughters occurring before ^{214}Bi - ^{214}Po delayed coincidences are vetoed; events must be reconstructed within the FV defined by the following conditions: $R \leq 3.021$ m and $|Z| \leq 1.67$ m where R is the reconstructed distance to the detector center and Z is the reconstructed vertical coordinate (the last condition excludes parts of the detector which observe higher than average event rates). The cuts reduce the live-time to 1270.6 days and the total FV exposure corresponds to 263.7 tonne \cdot y.

The model function fitted to the data has been restricted to the same components used in the solar neutrino analysis of the second phase (see [21]), namely ^{14}C , ^{85}Kr , ^{210}Bi β -decay shapes, the β^+ spectrum of the cosmogenic ^{11}C , the monoenergetic α peak from ^{210}Po decays, γ -rays from external sources and the electron recoil spectra from ^7Be , pp , pep and the CNO cycle neutrinos. Other backgrounds and solar neutrino components have a negligible impact on the total spectrum. Compared to previous solar neutrino analyses ([14, 22, 23, 26]) an extended energy region was used, including both pp and ^7Be neutrino contributions in the same fit. In addition, the upper threshold of the fit is set above the ^{11}C endpoint, which helps to constrain the resolution behaviour at the high end of the energy spectrum [21].

The analytical model used to describe the data is an improved version of the one described in [26] with the goal of enlarging the fitting energy range. The principal changes concern the non-linearities of the energy scale and the addition of the resolution parameter to take into account the low-energy region. The former parameters were first used in the pp -neutrino flux analysis [24]. The energy estimator N_p used is the number of PMTs triggered in each event (window of 230 ns) and is normalized to 2000 PMTs.

In the pp neutrino analysis (408 days of data) non-normalized energy variables were used, but normalization was introduced as the number of live PMTs began to drop significantly. In order to correct for the non-statistical fluctuations in the data from rebinning an intrinsically integer variable N_p a correction at each bin was applied, calculated on the basis of the known number of functioning PMTs at each moment. The model is discussed in [21], and more detail will be presented in a devoted paper [27].

The analytical model function has in total 15 free parameters. The free parameters describing the energy scale and resolution are the light yield and two resolution parameters: one takes into account the spatial non-uniformity of the detector's response and is relevant for the high-energy part of the spectrum and the other is responsible for the intrinsic resolution of the scintillator and effectively takes into account other contributions to the scintillation response width at low energies. Other parameters describe the rates of dominant backgrounds, namely ^{14}C (constrained to the value determined by analyzing an independent sample of ^{14}C events selected with low threshold, see [24] for more detail), ^{85}Kr , ^{210}Bi , ^{11}C ,

^{210}Po peak, and external backgrounds (responses from the ^{208}Tl and ^{214}Bi γ -rays modelled with MC). The pp and ^7Be interaction rates represent the solar neutrino parameters. The remaining free parameters describe the position and width of the ^{210}Po α -peak, and the starting point of the ^{11}C β^+ - spectrum (corresponding to 2 annihilation gammas of 511 keV) as independent calibration doesn't provide the necessary precision to have them fixed or constrained.

The pep and ^8B solar neutrino contributions were kept fixed according to the Standard Solar Model (SSM) predictions and the uncertainty of the prediction contributed to the systematics as described in section III. The minor contribution from external ^{40}K γ -rays was fixed too.

Other parameters of the model are tuned either using MC modeling or independent measurements and calibrations, for details see [21], [25] and [27]. They correspond to parameters describing the energy scale nonlinearities: the ionization quenching parameter, the contribution of the Cherenkov radiation, the geometric correction to the energy scale, the effective fraction of the single electron response under the threshold; and an additional parameter in the resolution description (quadratic with respect to the energy estimator). Special care is taken to describe the pile-up events. The same approach is adopted as the one developed for the pp -neutrino analysis [24], where the synthetic pile-up is constructed by overlapping real events with randomly sampled data of the same time length.

The ^{210}Bi background and the CNO neutrino spectra are strongly anticorrelated as they have similar spectral shapes. Their sum is constrained by the total number of events in the region between the ^7Be Compton-like shoulder and the ^{11}C spectrum (see Fig. 1), which is mostly free from other backgrounds. As the CNO contribution is masked by the larger ^{210}Bi rate, the CNO neutrino rate is fixed to the SSM+MSW prediction without considering electromagnetic contribution. We used both high and low metallicity variants of the SSM, the difference in results was included in the systematics. The electromagnetic term did not affect the fit results with respect to the CNO contribution as it was absorbed by the ^{210}Bi component.

The likelihood profile as a function of μ_ν^{eff} is obtained from the fit with the addition of the electromagnetic component for ^7Be and pp -neutrinos keeping μ_ν^{eff} fixed at each point. The electromagnetic contribution from all other solar neutrino fluxes is negligible and is not considered in the fit. Including the electromagnetic component described by (2) in the pp -neutrino cross-section leads to a decrease of the pp -neutrino flux in the fit, compensating for the increase in the total cross section. Another important correlation arises from the presence of ^{85}Kr in the fitting function. An increase in the ^7Be rate due to the electromagnetic interactions is compensated for by a decrease in the ^{85}Kr counting rate. These two correlations in the fit decrease the overall sensitivity to the magnetic moment. The contribution from ^{85}Kr could be

constrained from an independent measurement using a delayed coincidence, but the combination of a very low branching ratio of 0.4%, low tagging efficiency ($\sim 18\%$), and a relatively low ^{85}Kr rate lead to very low statistics in the coincidence branch [21]. As a result, constraining ^{85}Kr doesn't improve the sensitivity. On the other hand, the correlation between the magnetic moment and the pp -neutrino flux can be constrained by applying the results from radiochemical experiments, which are independent to the electromagnetic properties of neutrinos, to the sum of the neutrino fluxes detected in Borexino.

The radiochemical constraints are based on the results from [28]. The measured neutrino signal in gallium experiments expressed in Solar Neutrino Units (SNU) is:

$$R = \sum_i R_i^{Ga} = \sum_i \Phi_i \int_{E_{th}}^{\infty} s_i^{\odot}(E) P_{ee}(E) \sigma(E) dE =$$

$$= \sum_i \Phi_i < \sigma_i^{\odot} > = 66.1 \pm 3.1 \text{ SNU}, \quad (3)$$

where R is the total neutrino rate, R_i is the contribution of the i -th solar neutrino flux to the total rate, Φ_i is the neutrino flux from i -th reaction, $s_i^{\odot}(E)$ is the shape of the corresponding neutrino spectrum in the Sun, $P_{ee}(E)$ is the electron neutrino survival probability for neutrinos with energy E , and $\sigma(E)$ is the total cross-section of the neutrino interaction with Ga which has a threshold of $E_{th}=233$ keV.

If applied to Borexino the radiochemical constraint takes the form:

$$\sum_i \frac{R_i^{Brex}}{R_i^{SSM}} R_i^{Ga} = (66.1 \pm 3.1 \pm \delta_R \pm \delta_{FV}) \text{ SNU} \quad (4)$$

where the expected gallium rates R_i^{Ga} are estimated using new survival probabilities of P_{ee} based on recent values from [?] (therefore giving a new estimate for $< \sigma_i^{\odot} >$), $\frac{R_i^{Brex}}{R_i^{SSM}}$ is the ratio of the corresponding Borexino measured rate to its SSM prediction within the MSW/LMA oscillation scenario. We used the same SSM predictions for Borexino and the gallium experiments to avoid rescaling the gallium expected rates. The total deviation from the measured value should naturally include the additional theoretical error $\delta_R \simeq 4\%$ from the uncertainty in estimating the single rates contributing to the gallium experiments, and the uncertainty of the Borexino FV selection $\delta_{FV} \simeq 1\%$.

Applying the radiochemical constraint (4) to the fit as an additional penalty term the analysis of the likelihood profile gives a limit of $\mu_{\nu}^{eff} < 2.6 \cdot 10^{-11} \mu_B$ at 90% C.L. for the effective magnetic moment of neutrinos using the "standard" fit conditions (230 ns time window energy variable, synthetic pile-up, high metallicity SSM and fixing the energy scale and resolution parameters). Without radiochemical constraints the limit is weaker $\mu_{\nu}^{eff} < 4.0 \cdot 10^{-11} \mu_B$ at 90% C.L. and is not used in the present analysis. An example of the spectral fit is presented in Fig. 1.

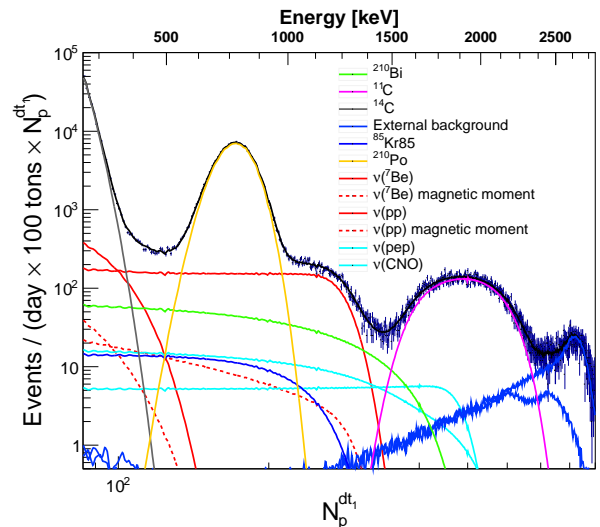


FIG. 1. Spectral fit with the neutrino effective moment fixed at $\mu_{\nu}^{eff} = 2.8 \times 10^{-11} \mu_B$ (note the scale is double logarithmic to underline the contributions at lower energies).

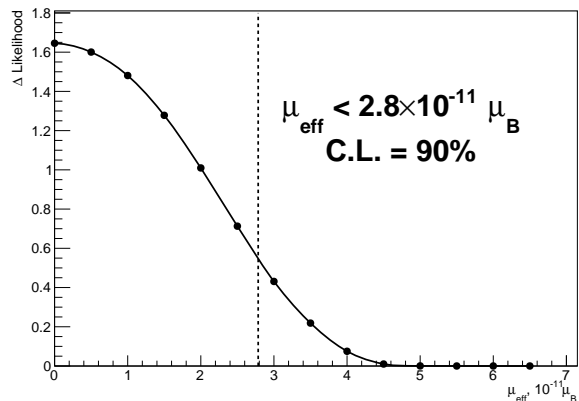


FIG. 2. Resulting weighted likelihood profile used to estimate the limit on the neutrino magnetic moment. The profile doesn't follow the gaussian distribution as it is flatter initially and goes to zero faster than the normal distribution. The limit corresponds to 90% of the total area under the curve. Note that unphysical values of $\mu_{\nu}^{eff} < 0$ are not considered.

III. SYSTEMATICS STUDY

The systematics have been checked following the approach developed for other Borexino data analyses [24, 29]. The main contributions to the systematics comes from the difference in results depending on the choice of energy estimator and the approach used for the pile-up modelling. The energy estimators used in the analysis are the number of PMTs triggered within a time window of 230 and 400 ns. The pile-up can be reproduced by either convolving the model spectra with the data acquired from the random trigger in the corresponding time win-

dow or by constructing a synthetic spectral component as described in [24]. Since the *pep*- and CNO- neutrino rates are fixed to the SSM predictions, the different rates corresponding to high/low metallicity models are also accounted for in the systematics. Further study included varying the fixed parameters within their expected errors.

The resulting likelihood profile is the weighted sum of the individual profiles of each fit configuration. Initially, the same weights are used for the pile-up and SSM choice, assuming equal probabilities for all 4 possibilities. Further weights are assigned proportionally to the maximum likelihood of each profile, therefore taking into account the quality of the realization of the model with a given set of parameters. Accounting for the systematic uncertainties the limit on the effective neutrino magnetic moment reduces to $\mu_{\nu}^{eff} < 2.8 \cdot 10^{-11} \mu_B$ at 90% C.L. The corresponding likelihood profile is shown in Fig. 2.

IV. MASS EIGENSTATES BASIS

Since neutrinos are a mixture of mass eigenstates the effective magnetic moment for neutrino-electron scattering is:

$$\mu_{eff}^2 = \sum_j \left| \sum_k \mu_{kj} A_k(E_\nu, L) \right|^2, \quad (5)$$

where μ_{jk} is an element of the neutrino electromagnetic moments matrix and $A_k(E_\nu, L)$ is the amplitude of the k -mass state at the point of scattering [30]. For the Majorana neutrino, only the transition moments are non-zero, while the diagonal elements of the matrix are equal to zero due to CPT-conservation. For the Dirac neutrino, all matrix elements may have non-zero values. The effective magnetic moment can be expanded both in terms of the mass eigenstates (this is more natural) or the flavor eigenstates. Under the assumption that $\theta_{13} = 0$, the form of the effective magnetic moment for the MSW oscillation solution has been investigated in [5, 31]. The analysis of Majorana transition neutrino magnetic moments taking into account the non-zero value of the angle θ_{13} was first performed in [33].

In the general case the expression for the effective magnetic moment in the mass eigenstate basis will have a complex form consisting of interference terms $\propto \mu_{jk}\mu_{ik}$. Without significant omissions the solar neutrinos arriving at the Earth can be considered as an incoherent mixture of mass eigenstates [5, 34]. In the case of Dirac neutrinos assuming that only diagonal magnetic moments μ_{ii} are non-vanishing:

$$\mu_{eff}^2 = P_{e1}^{3\nu} \mu_{11}^2 + P_{e2}^{3\nu} \mu_{22}^2 + P_{e3}^{3\nu} \mu_{33}^2 \quad (6)$$

where $P_{ei}^{3\nu} = |A_i(E, L)|^2$ is the probability of observing the i -mass state at the scattering point for an initial electron flavor.

In the case of Majorana transition magnetic moments the effective moment is:

$$\mu_{eff}^2 = P_{e1}^{3\nu} (\mu_{12}^2 + \mu_{13}^2) + P_{e2}^{3\nu} (\mu_{21}^2 + \mu_{23}^2) + P_{e3}^{3\nu} (\mu_{31}^2 + \mu_{32}^2) \quad (7)$$

For the well known approximation of three- to two-neutrino oscillation probabilities for solar neutrinos [5]: $P_{e1}^{3\nu} = \cos^2 \theta_{13} P_{e1}^{2\nu}$, $P_{e2}^{3\nu} = \cos^2 \theta_{13} P_{e2}^{2\nu}$ and $P_{e3}^{3\nu} = \sin^2 \theta_{13}$ – one can get the effective magnetic moment expressed in well-established oscillation parameters in the mass eigenstate basis. Equation (6) can be rewritten as:

$$\mu_{eff}^2 = C_{13}^2 P_{e1}^{2\nu} \mu_{11}^2 + C_{13}^2 P_{e2}^{2\nu} \mu_{22}^2 + S_{13}^2 \mu_{33}^2 \quad (8)$$

where $C_{13}^2 \equiv \cos^2 \theta_{13}$ and $S_{13}^2 \equiv \sin^2 \theta_{13}$, and $P_{e1}^{2\nu} + P_{e2}^{2\nu} = 1$. Similarly, assuming CPT-conservation ($\mu_{jk} = \mu_{kj}$) relation (7) for the transition moments can be rewritten as:

$$\mu_{eff}^2 = C_{13}^2 P_{e1}^{2\nu} \mu_{12}^2 + (1 - C_{13}^2 P_{e2}^{2\nu}) \mu_{13}^2 + (1 - C_{13}^2 P_{e1}^{2\nu}) \mu_{23}^2 \quad (9)$$

In general, $P_{e1}^{2\nu}$ and $P_{e2}^{2\nu}$ (and $P_{ee}^{2\nu}$) depend on the neutrino energy and shape of the neutrino spectrum (*pp*, ${}^7\text{Be}$, ${}^8\text{B}$ etc.), but in the energy region below 1 MeV, a dominant contribution to the recoil-electron spectrum comes from *pp*, ${}^7\text{Be}$, and CNO neutrinos, for which dependence of $P_{e1}^{2\nu}$, $P_{e2}^{2\nu}$ and $P_{ee}^{2\nu}$ on energy is weak and the probabilities can be assumed constant. Under such assumptions, since μ_{eff}^2 is the sum of positively defined quantities, one can constrain any term in (8) and (9). By using the most probable values of $P_{ee}^{2\nu}$, θ_{13} and θ_{23} [18] one can obtain the following limits from the relation $\mu_{eff} \leq 2.8 \times 10^{-11} \mu_B$:

$$|\mu_{11}| \leq 3.4; \quad |\mu_{22}| \leq 5.1; \quad |\mu_{33}| \leq 18.7; \quad (10)$$

$$|\mu_{12}| \leq 2.8; \quad |\mu_{13}| \leq 3.4; \quad |\mu_{23}| \leq 5.0; \quad (11)$$

all measured in units of $10^{-11} \mu_B$ and for 90% C.L..

V. LIMITS ON MAGNETIC MOMENTS OF THE NEUTRINO FLAVOR STATES

The effective magnetic moment for the LMA-MSW solution is (assuming the survival probability of *pp* and ${}^7\text{Be}$ solar neutrinos is the same):

$$\mu_{eff}^2 = P^{3\nu} \mu_e^2 + (1 - P^{3\nu}) (\cos^2 \theta_{23} \mu_\nu^2 + \sin^2 \theta_{23} \mu_\tau^2), \quad (12)$$

where $P^{3\nu} = \sin^4 \theta_{13} + \cos^4 \theta_{13} P^{2\nu}$ is the probability that ν_e is detected in its original flavor (survival probability), with $P^{2\nu}$ calculated in the ‘‘standard’’ 2-neutrino

scheme, θ_{13} and θ_{23} are the corresponding mixing angles. Though $P^{2\nu}$ depends on E_ν , the difference between $P^{2\nu}(400) = 0.57$ for a neutrino energy close to the pp -neutrino spectrum end-point of 420 keV (only a small fraction of the total pp -neutrino spectrum close to the end-point contributes to the sensitive region in our analysis) and $P^{2\nu}(862) = 0.55$ for ${}^7\text{Be}$ -neutrinos (higher energy line) is negligible and we can reasonably assume them equal. Moreover, tests performed by “turning on” separately the pp and ${}^7\text{Be}$ neutrino magnetic moments demonstrates that sensitivity to the magnetic moment is dominated by the ${}^7\text{Be}$ -neutrino contribution. Therefore an estimate of $P^{2\nu}(400) = 0.55$ is used in further calculations.

The limits on the flavor magnetic moment can be obtained from (12) because individual contributions are positive. With $\mu_\nu^{eff} < 2.8 \cdot 10^{-11} \mu_B$ and for $\sin^2 \theta_{13} = 0.0210 \pm 0.0011$ and $\sin^2 \theta_{23} = 0.51 \pm 0.04$ for normal hierarchy (or $\sin^2 \theta_{23} = 0.50 \pm 0.04$ for inverted hierarchy) [18] we obtain: $\mu_e < 3.9 \cdot 10^{-11} \mu_B$, $\mu_\mu < 5.8 \cdot 10^{-11} \mu_B$ and $\mu_\tau < 5.8 \cdot 10^{-11} \mu_B$, all at 90% C.L.

Because the mass hierarchy is still unknown, the values above were calculated for the “unfortunate” choice of hierarchy, providing conservative limits.

VI. CONCLUSIONS

New upper limits for the neutrino magnetic moments have been obtained using 1291.5 days of data from the Borexino detector. We searched for effects of the neutrino magnetic moments by looking for distortions in the shape of the electron recoil spectrum. A new model independent limit of $\mu_\nu^{eff} < 2.8 \cdot 10^{-11} \mu_B$ is obtained at 90% C.L. including systematics. The limit is free from uncertainties associated with predictions from the SSM neutrino flux and systematics from the detector’s FV and is obtained by constraining the sum of the solar neutrino fluxes using the results from gallium experiments. The limit on the effective neutrino moment for solar neutrinos was used to set new limits on the magnetic moments for the neutrino flavor states and for the elements of the neutrino magnetic moments matrix for Dirac and Majorana neutrinos.

VII. ACKNOWLEDGEMENTS

The Borexino program is made possible by funding from INFN (Italy), NSF (USA), BMBF, DFG, HGF and MPG (Germany), RFBR (Grants 16-02-01026A, 15-02-02117A, 16-29-13014 ofi-m, 17-02-00305A) and RSF (Grant 17-12-01009) (Russia), JINR Grant 17-202-01, and NCN Poland (Grant UMO-2013/10/E/ST2/00180). We acknowledge the generous hospitality and support of the Laboratory Nazionali del Gran Sasso (Italy).

-
- [1] M.B. Voloshin, M.I. Vysotskii and L.B. Okun, Sov.J. Nucl. Phys. 44, 440 (1986); Sov.Phys. JETP **64**, 446 (1986)
 - [2] C.S. Lim and W. Marciano, Phys. Rev. D **37**, 1368 (1988).
 - [3] E.Kh. Akhmedov, Phys. Lett. B **231** (1988)
 - [4] H.O. Back *et al.* (Borexino Collaboration) Phys. Lett. B **563**, 35 (2003)
 - [5] W. Grimus *et al.* Nucl. Phys. B **646**, 376 (2003)
 - [6] C.Giunti and A.Studenikin, Rev.Mod.Phys. **87**, 531 (2015).
 - [7] K. Fujikawa, R.E. Shrock Phys. Rev. Lett. **45**, 963 (1980).
 - [8] J. Schechter and J. W. F. Valle, Phys. Rev. D **24**, 1883 (1981).
 - [9] B. Kayser, Phys.Rev. D **26**, 1662 (1982).
 - [10] J. F. Nieves Phys. Rev. D **26**, 3152 (1982).
 - [11] P. B. Pal and L. Wolfenstein, Phys. Rev. D **25**, 766 (1982).
 - [12] R. E. Shrock, Nucl. Phys. B **206**, 359 (1982).
 - [13] D.W. Liu *et al.* (Super-KamiokaNDE Collaboration), Phys. Rev. Lett. **93**, 021802 (2004).
 - [14] C. Arpesella, *et al.* (Borexino Collaboration), Phys.Rev.Lett. **101**, 091302 (2008).
 - [15] A.G. Beda *et al.* (GEMMA Collaboration), Phys.Part. and Nucl.Lett. **10(2)**, 139 (2013).
 - [16] G.G. Raffelt and D.S.P. Dearborn, Phys. Rev. D **37**, 2 (1988).
 - [17] S. Arceo-Díaz, K.-P. Schröder, K. Zuber and D. Jack, Astropart. Phys. **70**, 1 (2015).
 - [18] C. Patrignani *et al.* (Particle Data Group), Chin. Phys. C, **40**, 100001 (2016) and 2017 update.
 - [19] G. Alimonti *et al.* (Borexino Collaboration) Nucl.Instrum.Meth.A **600**, 568 (2009).
 - [20] G. Alimonti *et al.* (Borexino Collaboration) Astropart. Phys. **16**, 205 (2002).
 - [21] M. Agostini, *et al.* (Borexino Collaboration) arXiv:1707.09279 (2017).
 - [22] G.Bellini *et al.* (Borexino Collaboration), Phys.Lett.B **658**, 101 (2008).
 - [23] G.Bellini *et al.* (Borexino Collaboration), Phys. Rev. Lett. **107**, 141302 (2011).
 - [24] G.Bellini *et al.* (Borexino Collaboration), Nature **512**, 383 (2014).
 - [25] M.Agostini *et al.* (Borexino Collaboration), arXiv:1704.02291 (submitted to Astrop.Phys.).
 - [26] G.Bellini *et al.* (Borexino Collaboration), Phys. Rev. D **89**, 112007 (2014).
 - [27] (Borexino Collaboration) in preparation (2017).
 - [28] J. N. Abdurashitov *et al.* (SAGE Collaboration) Phys. Rev. C, **80**, 1 (2009).

- [29] M. Agostini, *et al.* (Borexino Collaboration) Phys. Rev. Lett. **115**, 231802 (2015).
- [30] J.F. Beacom, P. Vogel, Phys. Rev. Lett. **83**, 5222 (1999).
- [31] A. Joshipura, S. Mohanty, Phys. Rev. D **66**, 012003 (2002).
- [32] S. Abe et al. (KamLAND Collaboration) Phys.Rev.Lett. **100**, 221803, (2008).
- [33] B.C. Cañas, O.G. Miranda, A. Parada, M Törtola and J.W.F. Valle, Phys. Lett. B **753**, 191 (2016); Addendum: Phys. Lett. B **757**, 568 (2016).
- [34] A.S. Dighe, Q.Y. Liu and A.Yu. Smirnov, hep-ph/9903329.